Q. Jl R. astr. Soc. (1968) **9**, 13–39.

The Theory of Cepheid Variability

R.F.Christy

(George Darwin Lecture, delivered at Burlington House on 1967 September 8)

INTRODUCTION

It is now just 50 years since Eddington's first paper on Cepheid pulsation (1). He recognized immediately the central problem of the maintenance of pulsation and proceeded to develop (2) the linear theory leading to the period–density relation. He continued to devote considerable attention (3) to understanding the physical mechanisms responsible for exciting pulsation and recognized all of the essential aspects of that problem.

His point of view on pulsation was expressed in *Stars and Atoms*: 'to be able to see the machinery of a star throbbing with activity is most instructive for the development of our knowledge'. This view constitutes the theme of the work I will discuss here on the application of non-linear methods to the Cepheid variables.

The discussion will be divided into three main parts, of which the first will be devoted to the methods of investigation. The second part will be aimed at understanding the physical causes of pulsation and the mechanism of amplitude limitation. The third part will discuss the various results of pulsation calculations. The objective of this part will be to find ways by which all the significant physical parameters (mass M, mean effective temperature T_{e0}, mean luminosity L_0, and helium mass fraction Y) that control pulsation can be deduced from observation of the variable star.

I. METHODS

The equations of motion

The equations of spherically symmetric motion are conveniently written (4) in a Lagrangian system where the mass $M(r)$ interior to r is the independent space variable. It is

$$M(r) = \int_0^r 4\pi r'^2 \rho(r')\, dr'$$

where $\rho(r)$ is the density. The equation of motion of an element of mass is

$$\frac{\partial^2 r}{\partial t^2} = -\frac{G\,M(r)}{r^2} - 4\pi r^2 \frac{\partial P(\rho,T)}{\partial M} \tag{1}$$

where G is the constant of gravitation and P is the pressure.

The radiative diffusion flux $L(r)$ passing radius r is

$$L(r) = -(4\pi r^2)^2 \frac{4\sigma}{3\kappa(\rho,T)} \frac{d(T^4)}{dM} \tag{2}$$

where σ is the Stefan–Boltzmann constant, $\kappa(\rho,T)$ is the opacity, shown in Fig. 1 for a typical case, and T is the temperature. The heat diffusion equation is then

$$T \frac{\partial S(\rho,T)}{\partial t} = -\frac{dL}{dM} + \epsilon(\rho,T) \tag{3}$$

where S is the entropy, and ϵ the nuclear energy source.

At the free surface ($r=R_0$), $M(r)=M$, we use the boundary condition $P=0$ in the equation of motion. The radiative boundary condition is

$$\left.\frac{d(T^4)}{d\tau}\right)_{\text{surface}} = \left.\frac{T^4}{\text{const}}\right)_{\text{surface}}$$

where τ is the optical depth. I have used the value 2/3 for the constant in order to simulate the results of the solution of the transport equation at a free surface.

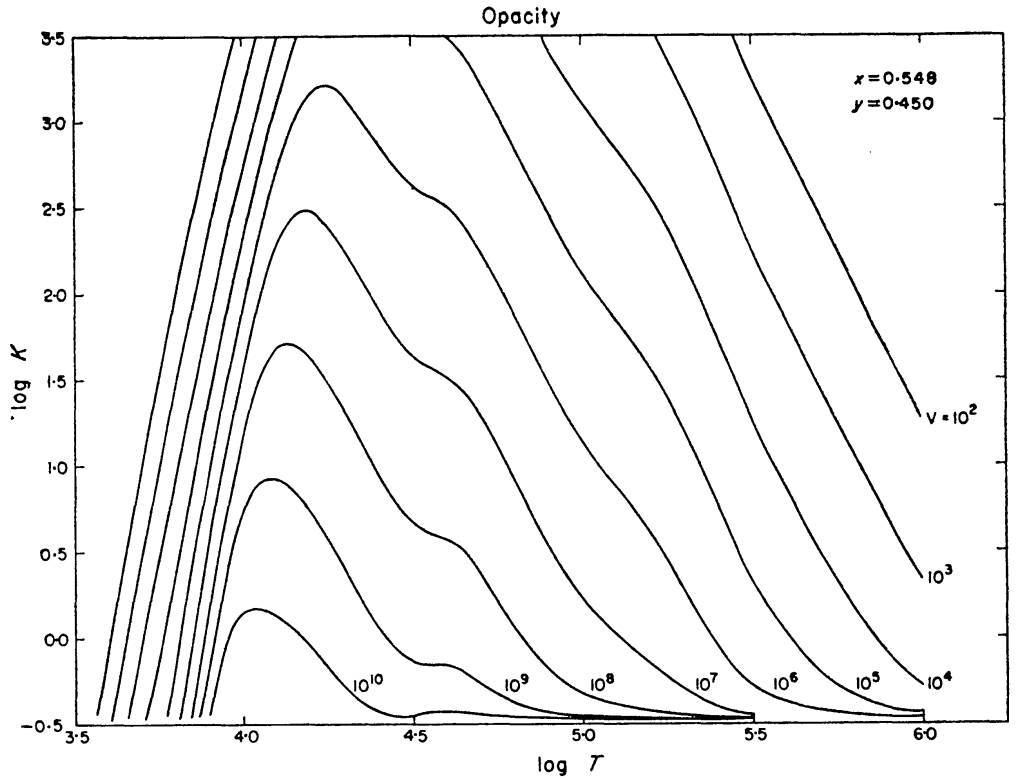

FIG. 1. The opacity as a function of temperature for various specific volumes from 10^2 to 10^{10}, 45 per cent helium and $Z=0{\cdot}002$.

For a giant star, because of the rapid increase in density near the core of the star, the amplitude of oscillation becomes very small inside $r=\frac{1}{4}R_0$. This permits the introduction of a rigid boundary at a small but finite inner radius which is outside the sources of stellar energy. There results the boundary condition $\dot{r}=0$ and $L=L_0$, the mean luminosity at this inner boundary. This elimination of the central region considerably simplifies the calculations.

The envelope structure

By setting time derivatives equal to zero in equations (1) and (3), we get equations which, together with the equation of state relating P, ρ, and T, describe the static structure of the stellar envelope. Because we are dealing with a giant type structure and are omitting the central core where most of the mass is concentrated, we do not need to satisfy the central conditions on a complete stellar model. In general, there is sufficient freedom in choosing the radius and molecular weight of a core to permit construction of a satisfactory stellar model for a wide range of envelopes that satisfy the above equations.

The envelopes are characterized by four parameters, M, L_0, either R_0 or T_{e0} and Y, the helium mass fraction. It was found earlier (5) that Z, the heavy element abundance, had little direct effect on pulsation; its principal effect is on the evolutionary history of the star and it thereby determines the appropriate values of the other parameters.

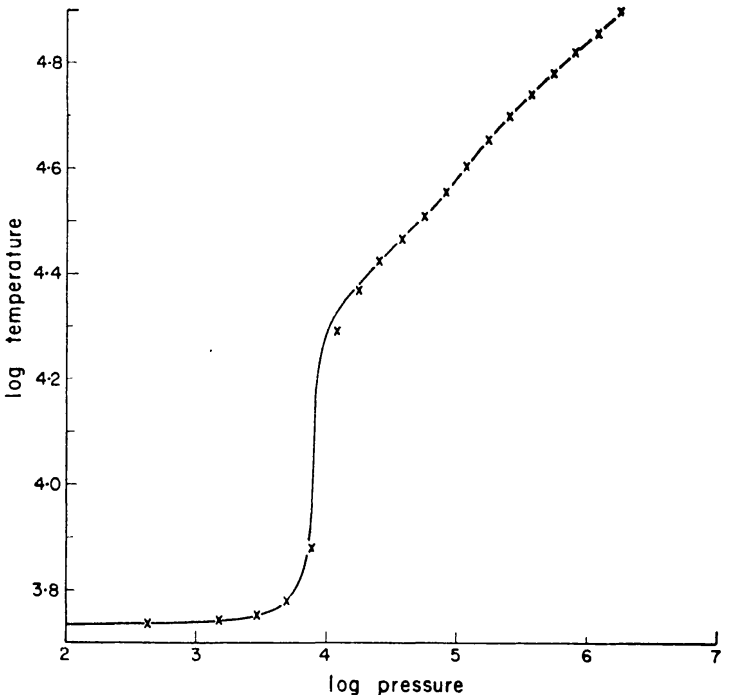

FIG. 2. The solid curve is the calculated run of T vs P for a radiative envelope with a fine mass division. The points x are calculated for a 38 mass zone envelope.

The principal features of the envelope structure are shown in Fig. 2. Below the photosphere, there is a very thin region near 10 000 °K where hydrogen becomes ionized and the temperature very rapidly rises. This region is, in general, convectively unstable but, because of the very low density in these envelopes, the convection is not effective in transporting heat at least near the high T_{e0} boundary of pulsation. It is ignored in the calculations reported here.

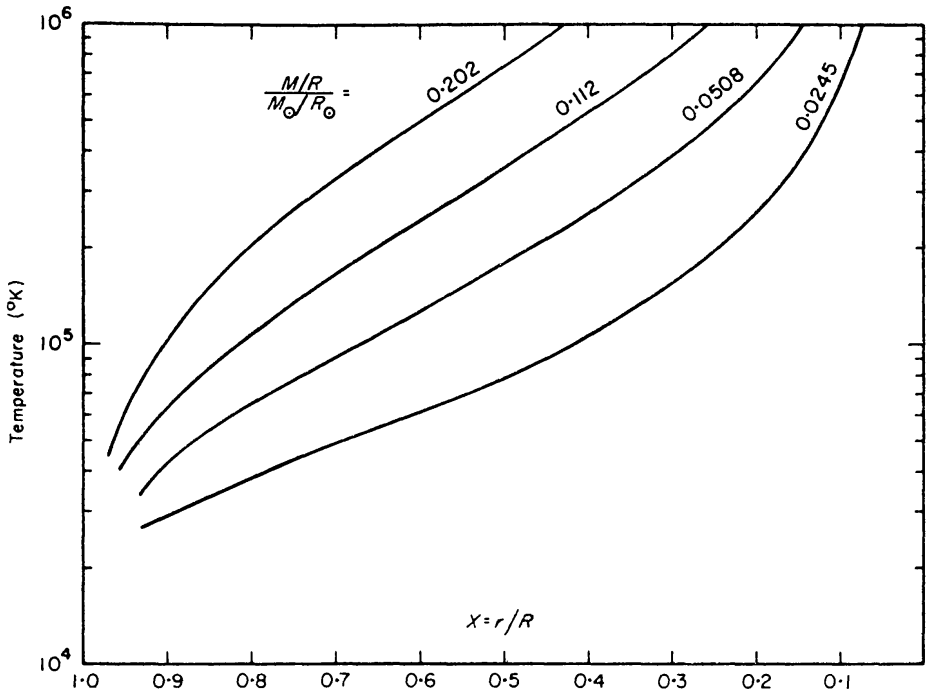

FIG. 3. The run of temperature vs $x=r/R$ for four envelopes with $(M/R)/(M_\odot/R_\odot)=0{\cdot}202$, 0·112, 0·0508, 0·0245.

At greater depth, the structure approximates a polytrope $\rho \sim T^n$ with $n \approx 3{\cdot}6$ for $T > 40\,000$ °K. The most significant way in which the various envelope structures differed was in the rate of increase of temperature with depth. Fig. 3 shows the temperature structure of a variety of envelopes. The significant parameter that distinguishes these envelopes is the ratio of mass to radius, M/R_0. The range over which pulsation has been investigated goes from $(M/M_\odot)/(R/R_\odot)=0{\cdot}019$, representing a model of W Vir, to $(M/M_\odot)/(R/R_\odot)=0{\cdot}20$, representing an attempt to study a δ Scuti variable. The present indications are that it is this parameter which primarily distinguishes the various classes of pulsating variables. Actually it has been found that a related parameter distinguishes even better the various types of pulsator. It is $V_{0.83} \equiv V(x=0{\cdot}83)$ where $V(x)$, defined by equation (5), is the ratio of gravitational to thermal energy. Apparently $x \approx 0{\cdot}83$, which is near the node of the first overtone, is the point in the envelope most charac-

teristic of the pulsation behaviour. The quantity $V(x)$ is shown in Fig. 4 for a variety of envelopes. Roughly, $V_{0.83} \propto \sqrt{M/R_0}$ for any given sequence of envelopes.

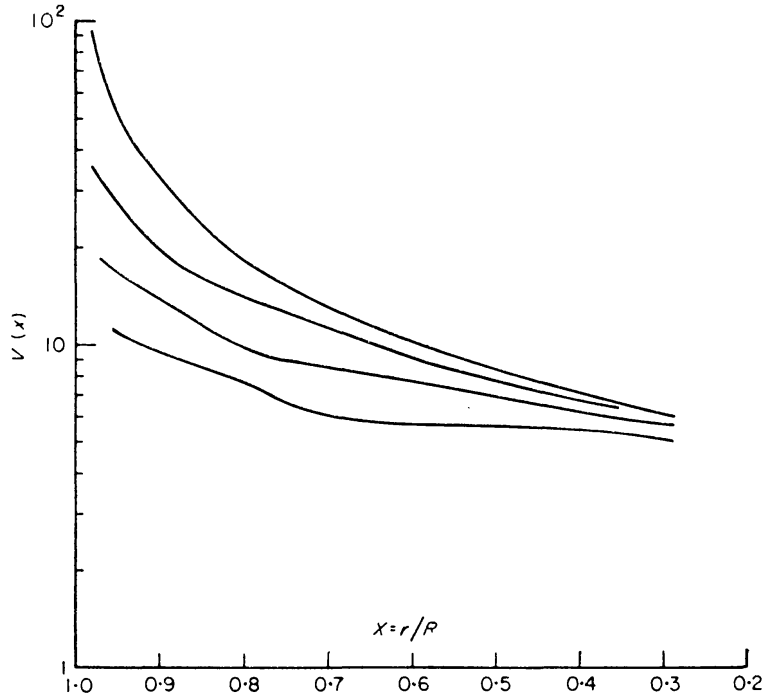

FIG. 4. The run of $V(x)$ vs $x=r/R$ for four envelopes. The values of $(M/R)/M_\odot/R_\odot)$ range from 0·202 for the topmost curve, through 0·075, 0·038, to 0·0245 for the lowest.

The linear calculations

Eddington's original treatment of pulsation considered the linearized equations resulting from the assumption of small, sinusoidal oscillations about equilibrium. In addition, an adiabatic assumption was made in which equation (3) is ignored and the deviations from equilibrium are assumed to be adiabatic with $\frac{\delta p}{p} = \gamma \frac{\delta \rho}{\rho}$.

If the deviation in radius is written $r=r_0\,(1+\xi(x,t))$ where $x=r_0/R_0$ and $\xi \sim e^{i\omega t}$, we get

$$\frac{d^2\xi}{dx^2} + (4 - V(x)) \frac{1}{x} \frac{d\xi}{dx} + \frac{V(x)}{x^2} \left[\frac{4-3\gamma}{\gamma} + \frac{x^3 R_0^3}{\gamma G M(x)} \omega^2 \right] \xi(x) = 0 \quad (4)$$

where

$$V(x) = \frac{\rho(x)\, G\, M(x)}{P(x)\, x\, R_0} \quad (5)$$

and G is the constant of gravitation. This equation, (4), is an eigenvalue equation for the frequency ω and leads to the amplitude function $\xi(x)$.

By considering the deviations from adiabatic behaviour arising from equation (3) as a perturbation, the rate of change of oscillation energy W can be determined. It is

$$\frac{dW}{dt} = \tfrac{1}{2} \int_0^M (\gamma - 1) \frac{\delta\rho}{\rho} (\delta\epsilon - \delta (dL/dM))\, dM \qquad (6)$$

which shows that the system can be excited or damped by the variation, during the oscillation, of the nuclear energy production or of the divergence of the radiation flux. For the giant stars of interest, the amplitude is too small near $x=0$, where the nuclear energy is produced, for a significant contribution from $\delta\epsilon$. The dependence of opacity κ on temperature and density throughout much of the envelope leads to a decrease of opacity on compression which implies a damping of vibration. It is only in the surface layers, where κ behaves differently and where the adiabatic assumption fails, that excitation can arise (**6**).

The first (**7**)–(**9**) clear indications of the excitation of pulsation were found in linear, non-adiabatic calculations in which small amplitude variations in equation (3) were treated simultaneously with equation (1). These calculations showed excitation arising primarily in the region of partial ionization of helium +. The absence of excitation in the hydrogen ionization region was due to inadequate treatment of this region and a subsequent calculation (**10**) showed a very large contribution from this zone.

The non-linear method

In order to treat better the surface regions of very large relative amplitude and to study the behaviour of an actual large amplitude variable star, non-linear calculations were initiated (**11**). In this method (**4**), (**12**), the envelope is divided into a series of spherical shells of carefully chosen relative mass. The equations of motion then became coupled differential equations for the motion and temperature variation of these mass shells. These coupled equations are then integrated numerically in time from some initial conditions. The radiation diffusion equation (3) was treated by an implicit differencing method to guarantee stability and the hydrodynamic equation (1) was treated by an explicit procedure in which the time step Δt was controlled by the Courant condition, which, for stability reasons, restricts Δt to a value less than the time for sound to cross a zone. An accurate equation of state and opacity law were used in tabular form.

The major problem in this calculation results from the steep temperature front near 10^4 °K which coincides with an important source of excitation in the star (see Fig. 2). Any attempt to use sufficiently fine zones to give an adequate description of this region leads to such short time steps that the calculation becomes impractical, requiring

about one hour on an IBM 7094, for one period of vibration. After considerable study, it was found that a description in terms of thick zones (considerably thicker than the front itself) could be used provided a transparency average, $\frac{2}{\kappa} \approx \frac{1}{\kappa_1} + \frac{1}{\kappa_2}$, of opacity of neighbouring zones was used. Actually, a somewhat more complicated average of this type was constructed to agree with exact integrations of the equation of heat flow on both sides of the front even for large differences of temperature. The points marked × in Fig. 2 show that this procedure was successful in integrating through the front with very few steps. This procedure is satisfactory only if the vibration amplitude is large enough so that the front crosses several zones in one period. For very small amplitude, the procedure is, in general, not precise and the excitation depends to some extent on the exact location of the front with respect to the coarse zones. In the problems of interest, the large amplitude condition was fulfilled with a description in terms of about 40 zones for the entire envelope. This permitted two time steps per second and about one period of vibration in one minute on an IBM 7094. The general temperature distribution in an equilibrium model is shown in Fig. 5. The zones were thin near the stellar surface and increased steadily (by about a factor ~1·4 in mass per zone) toward the interior. This permitted considerable detail (about 15 zones)

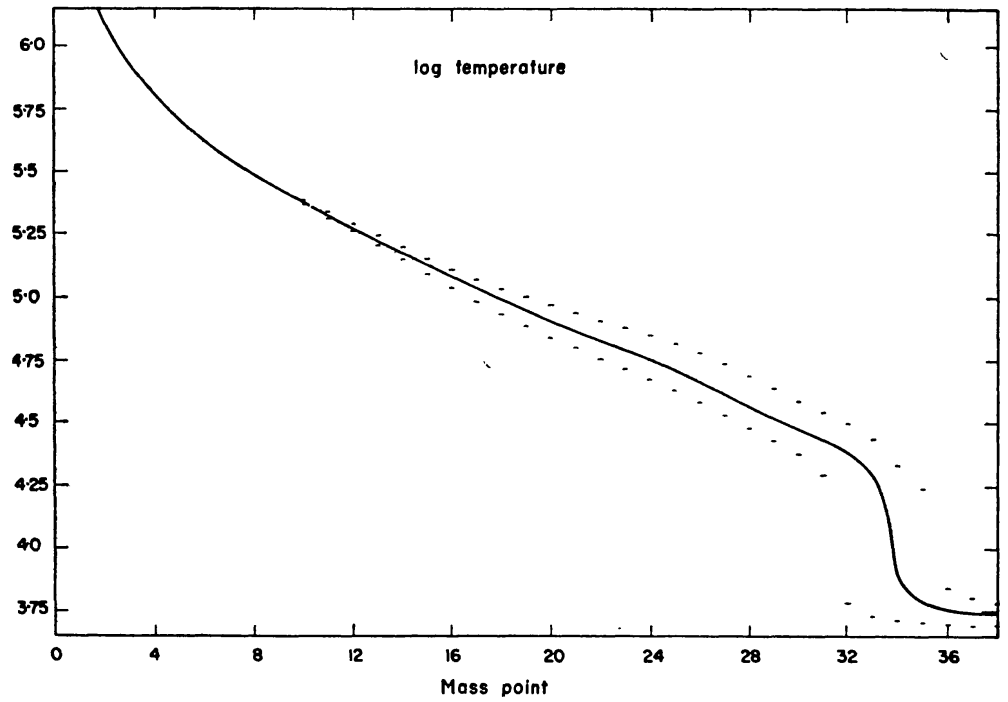

FIG. 5. The solid curve shows the temperatures of the 38 mass zones of a static envelope. The dashes show the extremes of temperature in the same envelope at maximum pulsation amplitude.

in the regions near the surface which cause the excitation, about 15 zones in the region of important dissipation, and about 10 further zones in the region of very small amplitude leading to the rigid boundary.

Temporal behaviour of the system

The system of equations was integrated numerically by first integrating the corresponding equilibrium equations in order to arrive at a static model for the initial condition of the dynamics. The usual method of initiating the dynamics was to superpose on the static model some prescribed initial run of velocities $\dot{r}(M)$. These initial velocities were usually chosen so as to approximate the velocities in a linear mode of vibration and with a large enough amplitude to minimize the time for the non-linear integrations.

Following initiation in this way, if the velocity distribution was well chosen, there results an approximately periodic vibration of the system which was found, for a stable model, to decay slowly in amplitude, or, for an unstable model, to grow slowly in amplitude. Together with the slow growth in amplitude, the solution also approximates better and better to periodicity as the unwanted modes contaminating the principal mode (usually the fundamental) slowly decay. After some growth in

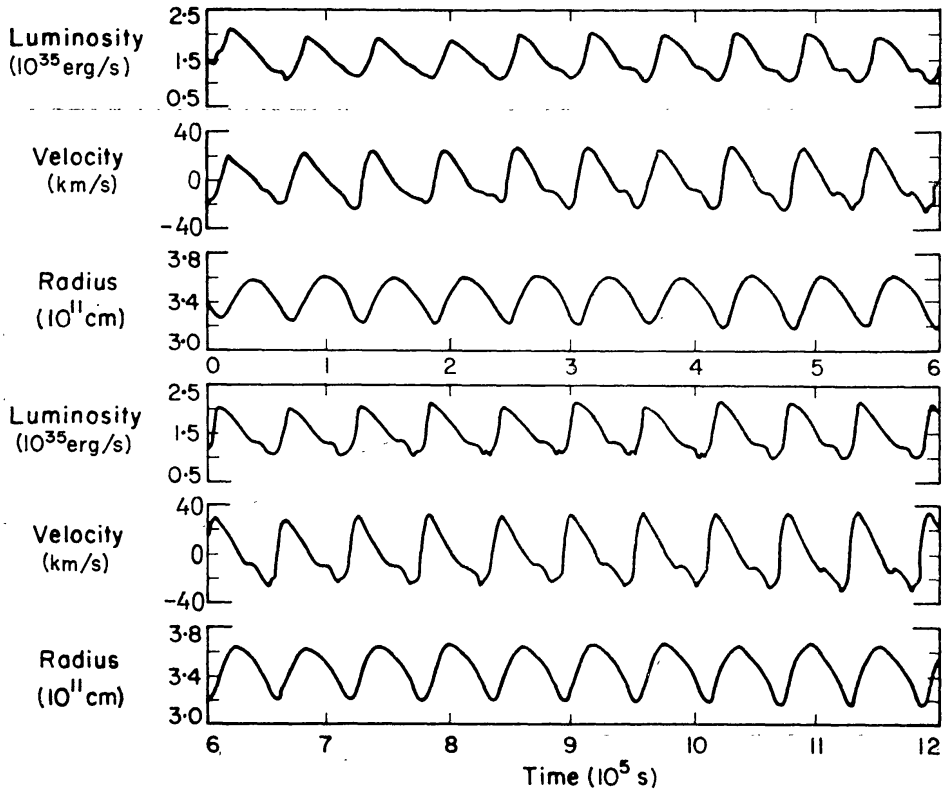

FIG. 6. The variation in time of the luminosity, surface velocity, and photospheric radius, for the first twenty periods of amplitude growth after initiation at intermediate amplitude.

amplitude (usually at least quadrupling the energy of vibration), the amplitude approaches an asymptotic limit characterizing the physical system (see Fig. 6). In this limit, the motion is non-sinusoidal throughout the star, even in the deep interior where the amplitude is small. Near the surface, the material velocities exceed sonic by a factor of 2 to 4 and shock waves may, in some cases, be seen. They were treated by the Von Neumann–Richtmyer artificial viscosity method.

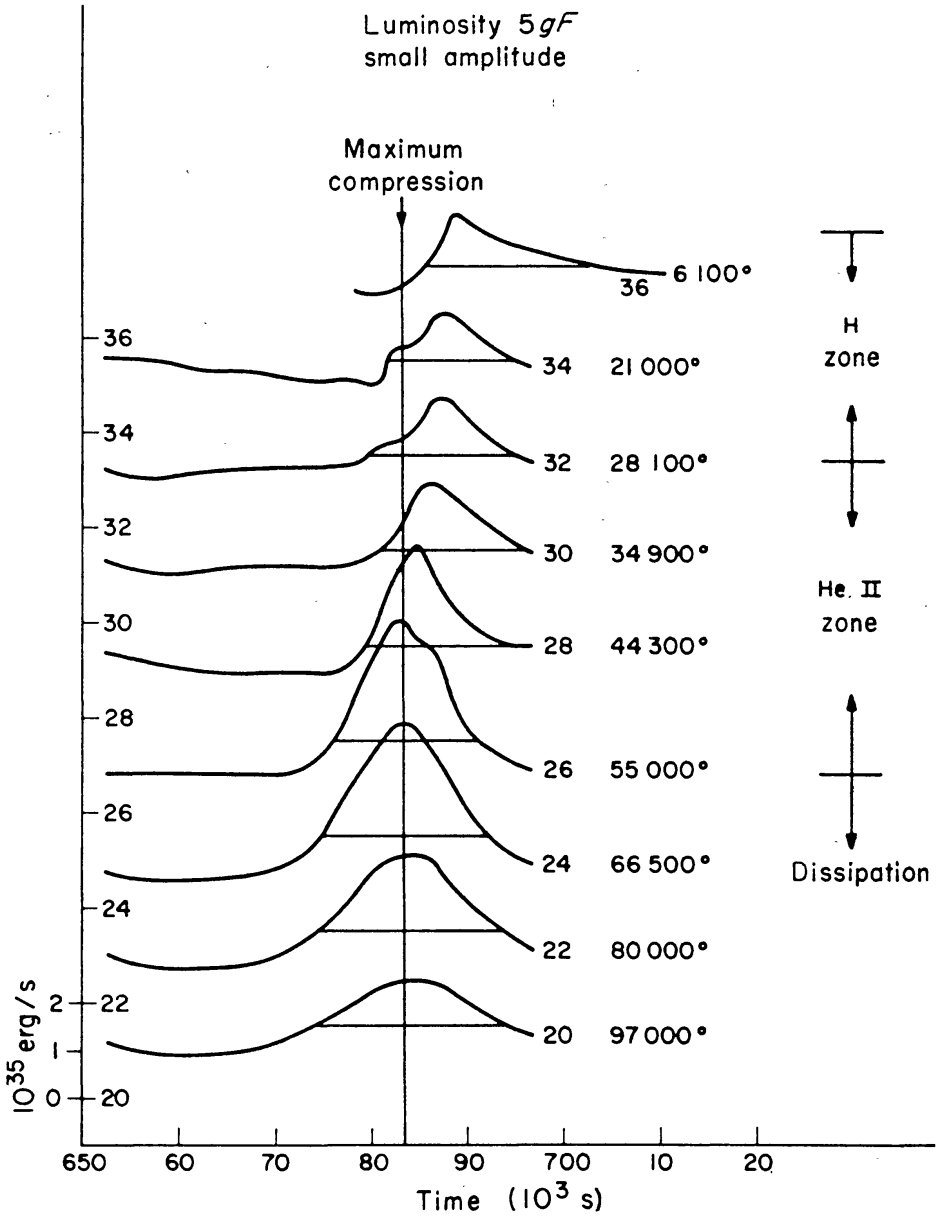

FIG. 7. The luminosity variation during one period at intermediate amplitude in the regions of maximum dissipation and of excitation. The amplitude, which is very large in the dissipation region, becomes diminished and delayed in the excitation region. Mean luminosity for each zone is shown by the horizontal line; the zero of scale for each zone is shown on the margin.

2. THE PHYSICAL BEHAVIOUR OF PULSATING STARS

The phase shift

The understanding and deduction of the phase shift has been a central problem of Cepheid variability from the earliest stages (1); even recent non-adiabatic linear calculations (10) have not settled the problem. These calculations found that the phase of the luminosity is delayed after minimum radius by only about 30° in the helium zone

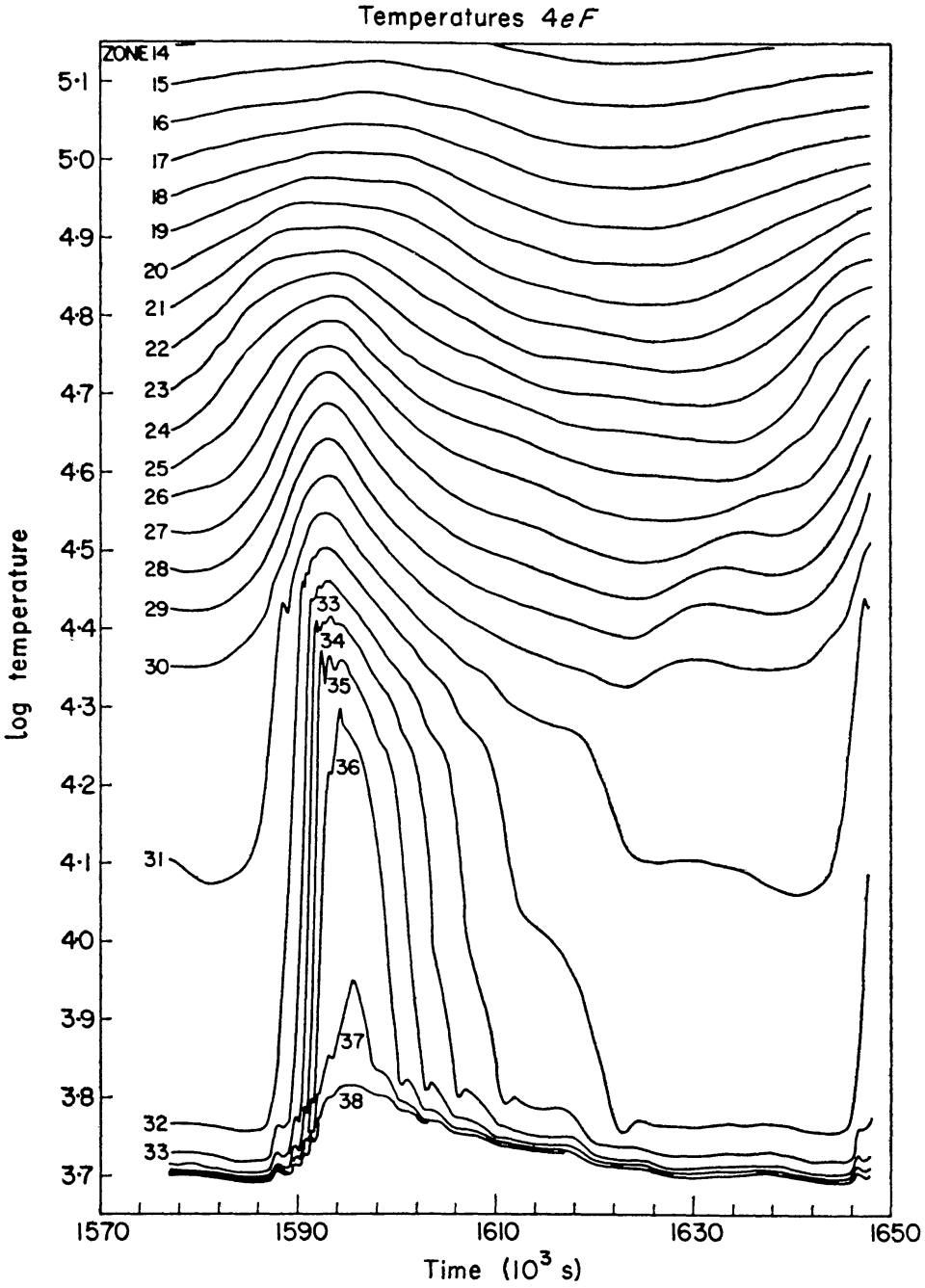

FIG. 8. The temperature variation in the outer envelope during one period at maximum amplitude.

and then is delayed by a very large amount in the hydrogen zone giving a total delay of about 180° at the surface. However, all the linear calculations of the behaviour of the hydrogen zone show such a large relative amplitude that it is clear that the results of the calculations are no longer meaningful even at amplitudes far smaller than those observed.

The non-linear calculations have followed the behaviour of the star, in particular of the surface layers, in the large amplitude region where the phase shift can be compared with observation (4), (5). The results agree with observation in the shape and phasing of the luminosity and

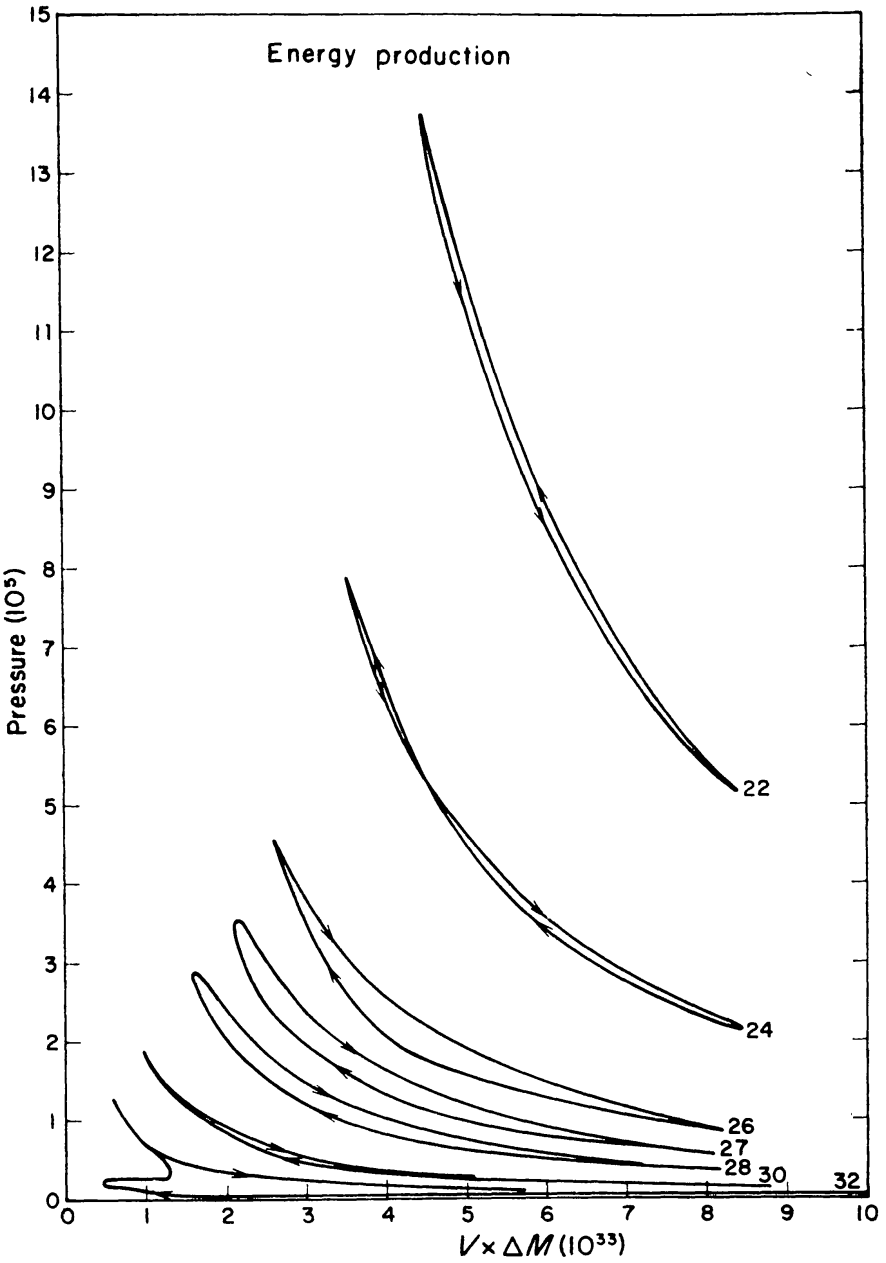

FIG. 9. *P–V* diagrams for selected zones.

velocity curves. Fig. 7 shows a sequence of luminosity curves at different depths. The progressive delay of peak luminosity in the helium zone amounts to about 30° or 1/10 period as in the linear theory. However, the change in the hydrogen zone is better described as a change in shape than as a large phase delay. The rising light phase becomes delayed and becomes very abrupt so that mean rising light comes near or sometimes slightly later than minimum radius. This is the '90° phase lag' but it really is not such a great lag in the centre of gravity of the main peak of the luminosity or in the positive phase of the luminosity. The calculated time of mean rising light comes very near minimum radius in most cases, as observed. The same phenomenon can be seen also in the set of curves in Fig. 8 showing the temperature dependence with time at various depths. Again, the main effect is a distortion of the time variation into a steep front in the hydrogen zone which then progressively eats through the surface of the star until the heat flux is released in the photosphere and then the same region progressively cools again until at maximum radius the photosphere reaches very deep into the star again.

The excitation of pulsation

In the non-linear calculations, the contribution of each layer to the excitation or dissipation has been found by examining P–V diagrams for each layer during one period. The area enclosed is the work per period, either positive or negative depending on the sense in which it is executed. Fig. 9 shows a sampling of such diagrams. Zone 22 shows nearly adiabatic motion but with dissipation; zones 26, 27, 28 show the excitation arising in the helium zone; the phase lag of the temperature rise has now given a considerable area to each loop which is executed with a significant departure from adiabaticity; zone 32 is an example of the behaviour in the hydrogen zone where there is a large excitation but no resemblance to adiabatic behaviour. These loops in the P–V diagram show how the delay in phase of maximum temperature after maximum compression is so closely related to the excitation of pulsation. The contribution of all zones (for a slightly different case) is shown in Fig. 10 where the separate, but comparable excitations due to the hydrogen zone and the helium zone are both apparent. At large amplitude, these zones nearly overlap so that there is actually no unambiguous definition of each.

The instability region

In view of the origin of the excitation in the hydrogen and helium zones very near the stellar surface, we can readily understand why the instability region is located near 6000° T_{e0}. It was found that the high T_{e0} boundary of instability is located so that the heat capacity to ionize

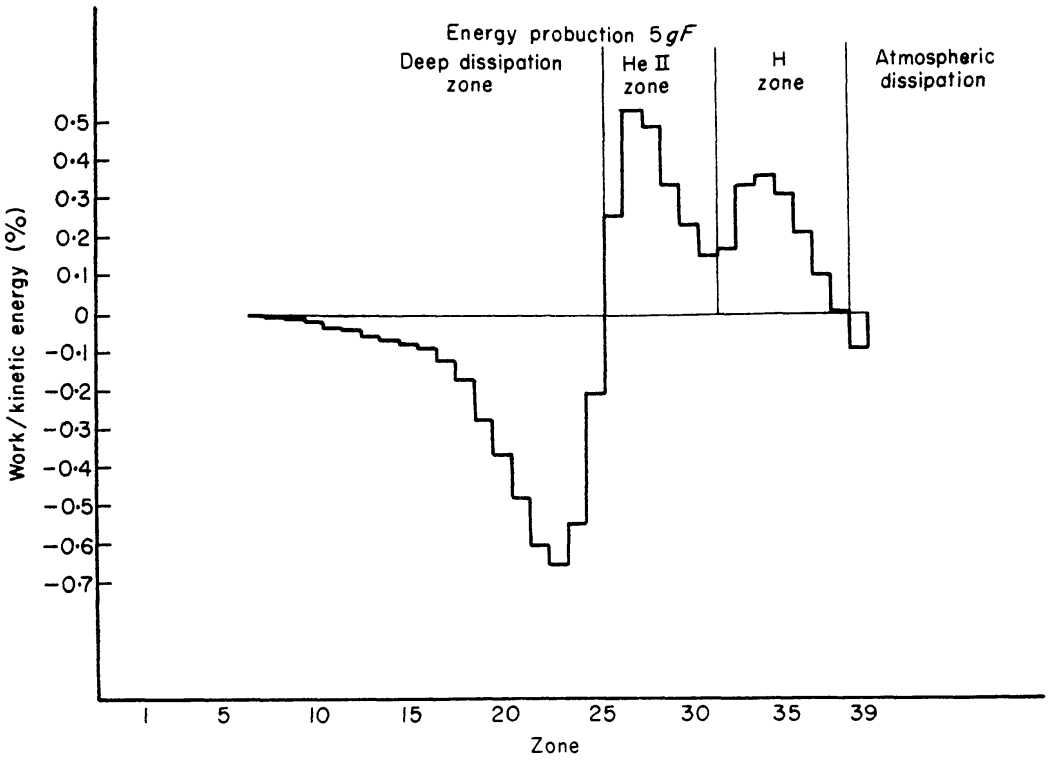

FIG. 10. The contribution of each zone during one period at maximum amplitude in per cent of the peak kinetic energy.

the unionized matter near the surface is just equal to the total heat flow from the star in 0·2 periods. In other words, there must be sufficient matter in these regions to be able to give a phase delay of about 0·2 periods, if the excitation is to be great enough to overcome the damping. For higher T_{e0} models, the heat capacity in the driving region is too small for effective action.

On the low T_{e0} side of the instability region, the contribution of the helium zone diminishes again as it becomes so deep that it behaves adiabatically and does not contribute effectively (**9**), (**15**). However, the behaviour of the hydrogen zone on the low T_{e0} side of the strip is still obscure. Linear, non-adiabatic calculations (**10**) continue to show significant driving due to hydrogen at lower T_{e0}. The non-linear calculations, on the other hand, have been unable, so far, to give satisfactory results for T_{e0} lower than ≈ 5300 °K since the coarse zone technique for the treatment of the hydrogen zone breaks down at such low T_{e0} that convection would be prominent. However, it is now generally believed that a time-dependent treatment of convection in the hydrogen zone is required, to understand the cessation of pulsational instability at the low T_{e0} boundary.

Physical mechanisms

The two mechanisms first recognized as important to pulsation were the nuclear reaction mechanism and the opacity mechanism. The first

depends on the rapid increase in nuclear rates with increasing temperature but is ineffective in most stars because of the very small amplitude of pulsation in the core of the star. The second mechanism is dissipative or exciting depending on whether the heat flux is increased or decreased on compression. If $\kappa \propto \rho^r/T^s$, the variation of opacity is

$$\frac{\delta\kappa}{\kappa} = [r-(\gamma-1)\,s]\,\frac{\delta\rho}{\rho}\,. \tag{7}$$

For the Kramers-type opacity with $r \approx 1$ and $s \approx 3$, this gives a decrease of opacity and an increase of heat flux on compression, unless γ is near 1, and thereby is responsible for the dissipation in much of the envelope. In an ionizing region, this effect may be reversed (7) since γ is near unity. However, there is another effect of an ionizing region (9), (15), which, even for a constant opacity, leads to excitation if the region is at a critical depth such that the pulsation is nearly adiabatic below the ionizing region whereas above the ionizing region there is too little heat capacity to control the flux. Then, on compression, the ionizing region stays cooler because of the small γ and thus absorbs extra heat from the deeper region at this phase and contributes excitation.

An additional peculiarity is also present in the helium + ionization zone (5). There is a small bump (Fig. 1) in the opacity near 40 000° associated with the coincidence of the Lyman edge of hydrogen and the peak in the Planck distribution. This bump introduces locally a significant reduction in s and can thereby also contribute excitation.

In and below the photosphere, to 20 000°, the opacity rises rapidly with temperature. It is this dependence which serves to delay the flux peak and, combined with the large heat capacity of ionizing hydrogen, leads to the absorption of heat at maximum compression and contributes the excitation in the hydrogen zone.

Although recent linear non-adiabatic and non-linear calculations have succeeded in finding the seat of instability by treating both the opacity and heat capacity in considerable and complicated detail, they have not automatically given a clear understanding of the cause of instability. In an attempt to clarify the various physical mechanisms, a number of models were calculated in which a modified opacity law was tried, or a modified helium content was used without correspondingly modifying the opacity law. The results of these calculations showed, however, a large interdependence of the various effects.

The two modifications tried were: first, modify the opacity law near 40 000 °K either to remove or augment the small bump. Second, the helium was removed from a model, modifying the heat capacity and γ in such a way that the opacity was not modified. For a model with no helium and no opacity bump, the excitation is all due to the hydrogen

zone which then becomes very important. Addition of helium adds excitation in the helium zone and diminishes it in the hydrogen zone. Addition of a bump at 40 000 °K but with no helium, also adds excitation in the helium zone and diminishes that in the hydrogen zone by an amount about equivalent to the effect of $Y=0{\cdot}1$. However, with considerable helium present, so the excitation is largely concentrated in the helium zone even with no bump, the addition of a bump in the opacity has very little effect. There is thus a strong interaction, as far as the excitation of pulsation is concerned, between the different parts of the envelope.

It seems clear, therefore, that all the various peculiarities in opacity and heat content which lie at $T<100\,000°$ can have significant influence on pulsation. Further, these effects are mutually interacting so that the final excitation of pulsation represents a composite phenomenon and is not readily dissectible into parts.

Comparison with linear non-adiabatic calculations

In order to explore the relation between the predictions of a linear non-adiabatic calculation and a non-linear calculation, I have made non-linear calculations for a series of models chosen to duplicate the series of δ Cephei evolutionary models published by Baker & Kippenhahn (**10**). The envelope structure of my models is almost identical with that of the Baker & Kippenhahn models with the exception of the hydrogen ionization zone, which in my model contains considerably less mass because of neglect of convection. This perturbation has no effect in and below the helium + ionization zone.

Most of the non-linear models were followed for about eight periods at 1/2 maximum amplitude using the opacity law I have used before (**5**). It was found that my periods were about 1 per cent shorter, and my instability region was shifted 500° to lower T_{e0}. I then noticed that the Baker & Kippenhahn opacity law differed from mine in having an opacity lower by about a factor of two in the temperature region below 45 000 °K. Although both sets of opacities are based on Los Alamos calculations, the Baker & Kippenhahn set was based on calculations not including the contribution of lines. This contribution raises the opacity in the region $T<50\,000°$ by a factor of about two.

I then modified my opacity law to match closely that of Baker & Kippenhahn and repeated a set of non-linear calculations at 1/2 maximum amplitude. The periods now were in accord with those of the linear calculation within the precision of their determination. The upper bound in T_{e0} for instability of the fundamental (at this amplitude) was now only 200 °K lower than that of Baker & Kippenhahn. The

upper bound in T_{e0} for instability in the first overtone was about 150 °K lower than that of Baker & Kippenhahn.

The only significant discrepancy with the results of the linear calculation came in the magnitude of the contribution of various regions of the star to excitation and dissipation. The contributions to the change in energy per period divided by the peak kinetic energy for the deep dissipating region, the helium + ionization zone, and the hydrogen ionization zone, were compared. In the large amplitude calculations, the dissipation region contributed a loss of between 4 and 5 per cent per period, whereas in the linear calculations this loss was only about 2 to 3 per cent per period (I have been informed by Baker that the figures given in (**10**) must be multiplied by 4π to agree with the above definition). The excitation contribution of the helium + zone was between 4 and 5 per cent with my usual opacity law and increased to 5 to 6 per cent with the Baker & Kippenhahn opacity, whereas the contribution in the linear calculation was only 1 to 3 per cent. The contribution of the hydrogen zone in my models was about 2 per cent, whereas it was 1 to 3 per cent in those of Baker & Kippenhahn. I repeated one model with finer zoning but there was no change in the results.

The different contributions of the two methods in the hydrogen zone were anticipated but the differences in the contributions in the helium + zone and the dissipation region were not anticipated and are somewhat greater than expected in view of the small amplitude of the non-linear models in those regions. The differences may reflect the effects, even deep in the envelope, of the different treatment of the hydrogen zone.

The maximum amplitude

In all cases, the non-linear calculations reach a maximum amplitude in the same range as is observed. The velocity amplitude and radius amplitude were similar to those observed as was the luminosity amplitude and the temperature amplitude. It was therefore of interest to explore the effects which control the limiting amplitude. In essentially all cases, the limiting amplitude was approached when the velocity curve began to show a very steep phase at minimum radius. When the duration of the outward acceleration phase had become very short, the amplitude stopped increasing.

In one case (**5**), a detailed investigation was made of the behaviour of the system in its approach to maximum amplitude. It appeared that the rapid acceleration occurred only in and above the helium zone. It is associated with the rapid expansion as the helium and hydrogen become ionized by the luminosity increase. This expansion leads to the rapid outward acceleration and a rapid increase in pressure and

temperature. These quantities become so high in the helium zone that the opacity drops and the flux leaks rapidly through the helium region causing the excitation due to this region to level off (Fig. 11). This levelling off of excitation then stops the increase of amplitude as the excitation then is just balanced by the dissipation.

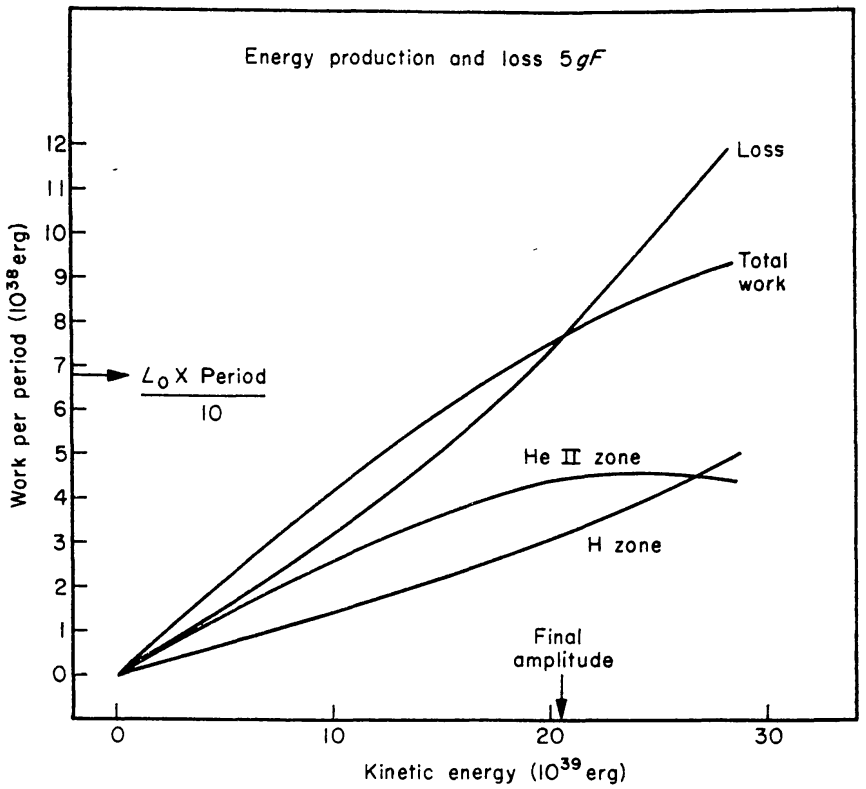

FIG. 11. The variation with amplitude of the excitation energy of the different regions, the total excitation energy, and the dissipation. The total excitation energy is comparable to 10 per cent of the energy radiated per period.

3. RESULTS OF PULSATION CALCULATIONS

Once we have achieved what seems to be a workable understanding of pulsating variables, we face two interrelated problems. On the one hand, we should now be able to account for all of the peculiarities and regularities in the observations of Cepheid-type variables. Correspondingly, we would like to be able to determine all of the four relevant parameters (M, L_0, T_{e0}, Y) from observation of a variable star. In this section, I will discuss the progress that has been made in this direction.

Systematics of luminosity and velocity curves, region of instability and periods

One set of investigations was made (5) on a series of RR Lyrae models to explore some measurable quantities that were not too sensitive to amplitude and which might be studied at somewhat less

than maximum amplitude. These quantities were: the phase delay of the luminosity curve relative to the velocity curve; a measure of the relative amplitude of velocity and light curves (actually the ratio $\mathscr{R}$ of the radius amplitude and the amplitude of the integral, $\int (L-L_0)\,dt$, of the positive phase of the luminosity curve was used); and the skewness of the luminosity curve as measured by the luminosity moment (the delay after mean light of the centre of gravity in time of the positive portion of the luminosity curve). The above quantities were chosen in order to minimize the uncertainties due to slight errors in shape and amplitude which are present in the calculated curves. The phase lag was defined as the delay of the instant of mean light during rising light after the instant of zero velocity at minimum radius.

It was found that the phase lag, the ratio $\mathscr{R}$ of relative radius amplitude to integrated luminosity amplitude, and the luminosity moment all increased in going from the high T_{e0} side to the low T_{e0} side of the instability region. This change in skewness toward less skew light curves was already known as the type *a* to type *b* change in RR Lyrae variables. Except for serving to distinguish overtone from fundamental modes, the quantities $\mathscr{R}$ and luminosity moment correlated well with each other and did not represent distinct observables. The phase lag seemed to be significantly larger for large Y than for small Y and could serve, together with one of the other measures, to determine Y as well as the location of the variable in the instability strip.

Of most immediate interest was the dependence of the high T_{e0} boundary of instability on the helium content Y. In a globular cluster, there are frequently enough variables to define this colour boundary quite well. If it is also possible to translate this observed colour into T_{e0}, it is possible to determine Y. The high T_{e0} boundary depends systematically on Y in such a way that the larger Y variables are unstable to higher T_{e0}. An approximate relation for this dependence is

$$\theta_{e0}\ (\text{high } T_{e0} \text{ boundary}) = 1{\cdot}09 - 0{\cdot}11 \log g - 0{\cdot}20\ Y.$$

The application to M3 with the boundary at $(B-V)_0 = 0{\cdot}17$ gave $Y = 0{\cdot}30$. Further work is necessary to verify this determination of T_{e0} and helium content and to apply this method to other clusters. The result is of considerable significance in the history of our Galaxy and also has an important bearing on the evolutionary history of the stars in question.

The periods of variables certainly provide the most precisely observed quantity and yield a very accurate relation between mass and radius. However, the pulsation constant $P\sqrt{\rho/\rho_\odot} = Q$ depends to some extent on the structure of the envelope. It was found that a quite accurate general expression for Q is $Q = 0{\cdot}22\ (V_{0{\cdot}83})^{-0{\cdot}60}$ which serves to describe

all the calculated periods. An alternative expression (**13**) in terms of M and R is not quite so precise and general, it is

$$Q = 0{\cdot}022\,(R/R_\odot)^{1/4}\,(M_\odot/M)^{1/4}\ .$$

Overtone behaviour

In the linear theory (**10**), the first radial overtone (and higher overtones) seem to show instability in essentially the same region as does the fundamental mode and with comparable growth rate. In contrast, the non-linear calculations, when initiated at medium amplitude, usually show growth in amplitude of either the fundamental or the first overtone but not both. The principal investigation of overtones has been in connection with RR Lyrae models (**5**), but a few examples have been investigated both of much longer periods (up to 20 days) and of much shorter period (down to 2 hr).

The general behaviour resulting from these investigations is that for models of large luminosity to mass ratio, the entire width of the instability strip is occupied at large amplitude by fundamental pulsators only. For low luminosity to mass ratio, the instability strip is entirely occupied at large amplitude by first overtone pulsators (higher overtones have not been explored). For intermediate luminosity to mass ratio, the high T_{e0} side of the instability region shows persistent pulsation in the first overtone, whereas the low T_{e0} side shows persistence of the fundamental.

It was found possible to characterize the overtone behaviour more simply in terms of the value of $V_{0{\cdot}83}$ of the envelope. For $V_{0{\cdot}83} > 19{\cdot}0$, large amplitude pulsation persists only in the first overtone, whereas for $V_{0{\cdot}83} < 19{\cdot}0$ large amplitude pulsation persists only in the fundamental, but it is not quite certain that this formulation of the dividing line is completely independent of luminosity. It is clear that the function $V(x)$ is very significant in determining the characteristics of large amplitude pulsation but a fuller explanation of this behaviour is still not available. Near the dividing line between these two kinds of behaviour, there were found a few models which could show persistent large amplitude pulsation in either the fundamental or the first overtone depending on the mode of initiation at intermediate amplitude. This clearly points to the final state of the system being dependent on its history in these cases.

A useful empirical relation was found to characterize the shortest period, P_{tr}, at which the pulsation would persist in the fundamental mode. Where this division was slightly obscure, as above, the centre of the transition region was chosen. This shortest period depended not on T_{e0} or on Y or on M, but only on L_0:

$$P_{tr} = 0{\cdot}057\,(L/L_\odot)^{0{\cdot}6}\ \text{days}\ .$$

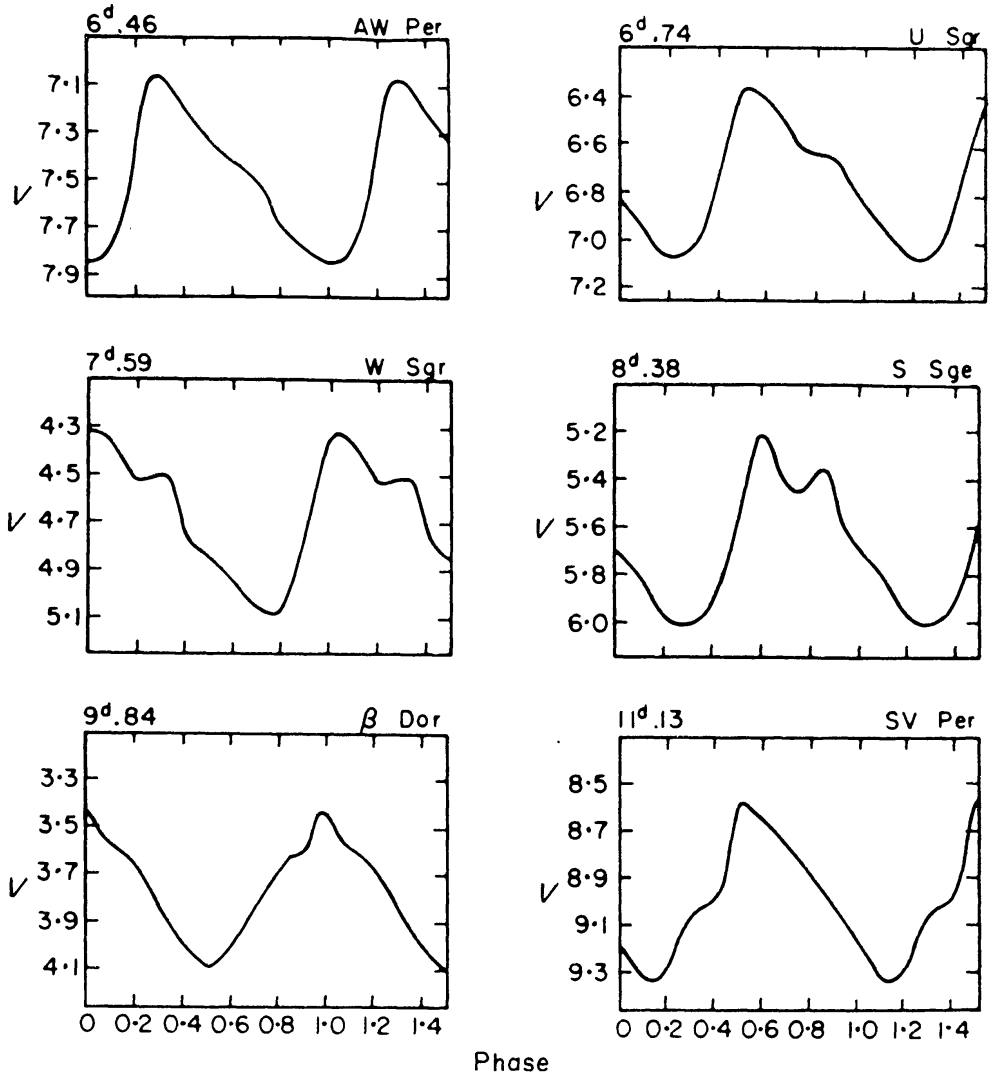

FIG. 12. Observed luminosity variation for six Cepheid variables. The curves are reproduced from Ref. (21).

This relation was primarily explored for RR Lyrae models but was found nearly correct even for $L/L_\odot$ as great as 2×10^4 and as small as 10. Since observation has shown such a boundary of fundamental pulsation only among RR Lyrae cluster variables,* it has been possible to apply this relation only there. This application led to $P_{tr}=0^d{\cdot}565$ in ω Cen and M15 giving $L/L_\odot=46$, whereas P_{tr} is $0^d{\cdot}496$ in M3 and $0^d{\cdot}455$ in M5 leading to $L/L_\odot=37$ and 32 respectively. These luminosities are in the same range as those deduced in other ways from observation but there is, as yet, no confirmation of the variation from cluster to cluster.

*However, a recent study (22) of the variables in the Small Magellanic cloud seems to show a new short period, small amplitude group of period 1 to 3·5 days, which may well represent the overtone group of Cepheids.

Secondary features in light and velocity curves

Among RR Lyrae variables, a second bump in the light curve at phase near 0·6 or 0·7 after mean rising light is sometimes quite visible. Among Cepheid variables, a second bump in the light curve is quite prominent in variables from 7 to 10 days or more (Fig. 12). It appears in this latter case that well-observed velocity curves show also a second bump (Fig. 13) which appears to correlate with that in the light curve in such a way that the second bump in light just precedes that in velocity. This feature of the light curve first becomes prominent for periods near 7 days at a phase about 0·45 after mean rising light and becomes progressively earlier and larger until at 10 days' period it becomes the maximum light and occurs at phase 0·25. For longer periods, the bump that had been peak light becomes a mere shoulder on the rising light and the second bump takes over the role of peak light. The shoulder disappears at about 20 days' period.

It had been found earlier in studying RR Lyrae models (5) that such a feature was commonly seen near phase 0·6 to 0·8 in the calculated velocity curve and also commonly in the light curve. In those cases it was noted that there was a minimum in T_{e0} and in L_0 at the time of the

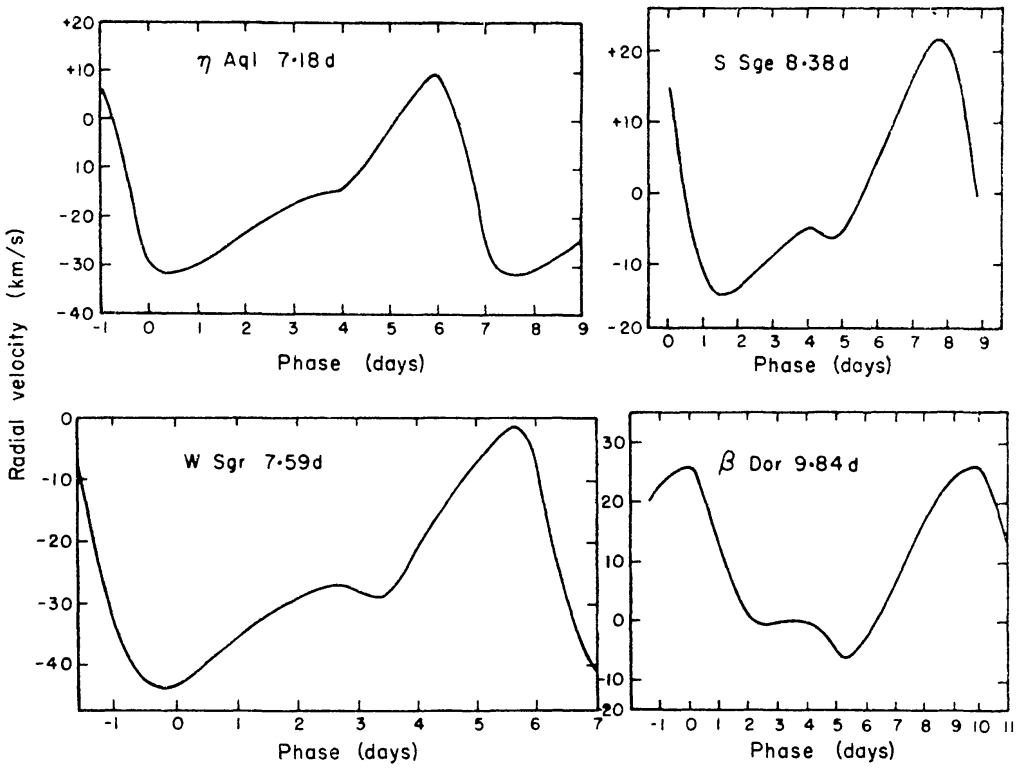

FIG. 13. Observed radial velocity variation in four Cepheid variables: η Aql and W Sgr from Jacobsen, T.S., 1926. *Lick Obs. Bull.*, **12**, 138. β Dor from Applegate, D., 1927. *Lick Obs. Bull.*, **13**, 12. S Sge from Herbig, G.H. & Moore, J.H., 1952. *Astrophys. J.*, **116**, 348

secondary outward acceleration because of an increase in opacity with compression which acted to reduce the flux. The bump in the light curve seemed to follow the minimum. The identification of this feature led to a choice of $M/M_{\odot}$ in the neighbourhood of 0·5 for these variables in order to get agreement with observation.

In the case of the Cepheids, there again appears to be a drop in T_{e0} and in L_0 at the time of the second outward acceleration but the secondary maximum in L_0 appears just to precede this drop rather than to follow it. Recently, I have made efforts to find what parameter choices in a model are necessary to reproduce a second outward acceleration at phase 0·3 to 0·5 as observed in the Cepheids. A number of models have been calculated and, as a result, I have found that a prominent second acceleration can arise in the models in the phase range 0·2 to 0·5 and this phasing can be correlated with the envelope structure as measured by $V_{0\cdot83}$ (Fig. 14).

In order to rely on this feature as an indicator of stellar properties, I examined the behaviour of certain models in detail in order to understand the origin of the feature. Fig. 15 shows the velocities of each zone in a 42-zone model during nearly two periods at maximum amplitude. The actual full amplitude of zone 42 (the outside surface) was 54 km/s, whereas that of zone 2 (the innermost) was 0·014 km/s. The velocity scale has been progressively shifted and enhanced by a factor reaching

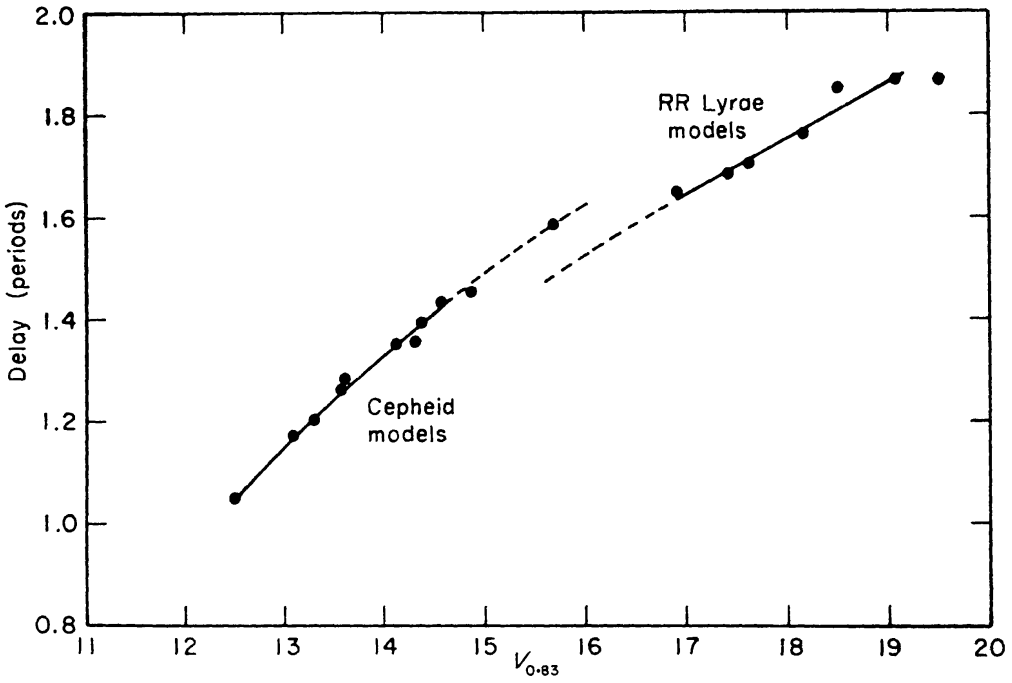

FIG. 14. The delay after zero radial velocity at minimum radius, of the subsequent secondary outward acceleration feature for a number of Cepheid models and a number of RR Lyrae models. The delays correlate with the envelope structure as measured by the quantity $V_{0\cdot83}$ (see equation (5)).

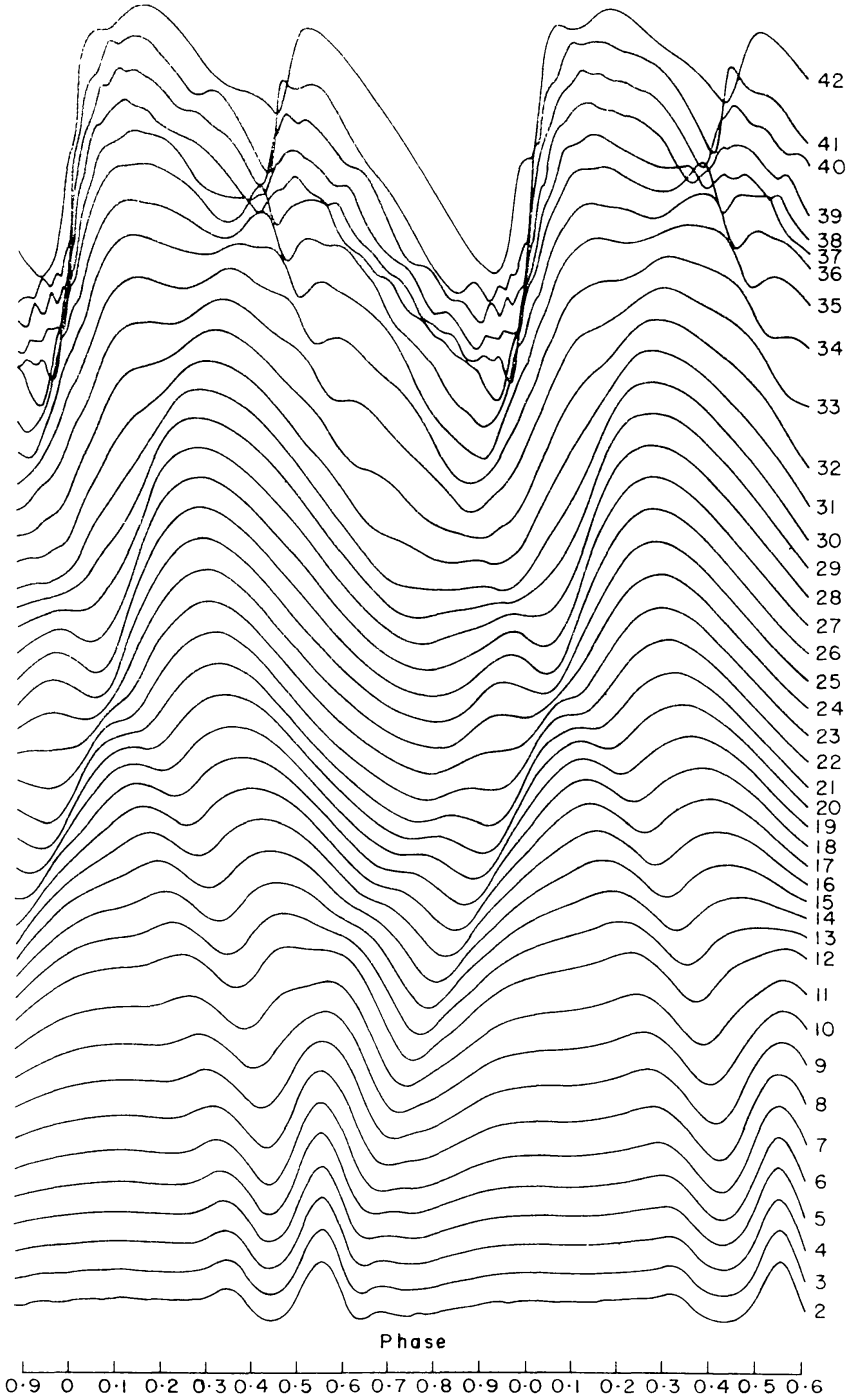

FIG. 15. Calculated velocities of all mass zones at maximum amplitude for a model stimulating β Dor. The zeros are progressively shifted and the scales progressively enhanced toward small radii (zone 2) in order to make visible the pattern of in and outgoing signals. Velocities outward from the star are plotted upward. The topmost curves refer to optical depths less than unity. Zone 2 is at $r/R=0{\cdot}1$.

1600 at zone 2 in order better to display the results. The radius of zone 2 is $\approx 0{\cdot}1$ of the outside radius and that of zone 6 is $\approx 0{\cdot}25$ of the outside radius. It is apparent that the character of the motion changes little in this range.

The general appearance of the velocities in the innermost zones is most surprising: it was commented on in the RR Lyrae calculations (**5**), (**14**). This impulsive behaviour was exceedingly strong in a calculated model of W Vir (**16**). A number of studies have been pursued to understand this behaviour. It has been found, for example, that this feature is not present at initiation and appears only after the first strong acceleration and large pressure peak appears in the outermost layers. When a signal has had time to propagate in to the centre, the impulsive behaviour starts. This and the signals that can be traced in Fig. 15 lead to the following picture: the large acceleration starting in the helium zone 33 at phase 0·9 sends a pressure pulse inward leading to the inward velocity of zone 2 at phase 0·45 and reflects from the central core as an outward velocity at phase 0·55 which, with an additional bounce at phase 0·65, propagates out to the surface at phase 0·45 as the secondary outward acceleration phase. Phases here are measured with respect to the primary outward acceleration at minimum radius. Thus the secondary bump is an echo of the primary bump 1·4 periods earlier. In addition to this echo phenomenon, there also appears to be a resonance phenomenon in that the ingoing and outgoing signals interfere with each other and sometimes reinforce and sometimes cancel. The result is that for some models the secondary bump is suppressed. In the case of the RR Lyrae models, bumps at phase 0·65 or greater, associated with $V_{0{\cdot}83}=17$ to 19·5, were strong. However, models with $15{\cdot}5 \leq V_{0{\cdot}83} \leq 17$ showed very small multiple bumps in the phase range 0·5 to 0·75. In the case of Cepheid models, only those with $12{\cdot}5 \leq V_{0{\cdot}83} \leq 15{\cdot}7$ have been examined carefully and particularly strong bumps were found for $13 \leq V_{0{\cdot}83} \leq 15$. A model with $V_{0{\cdot}83}=15{\cdot}7$ led to only a weak effect and one with $V_{0{\cdot}83}=17{\cdot}2$ showed none. Even this resonance phenomenon seems to correlate well with observation since the bump is strong for $7 \leq P \leq 11$ days, and seems to disappear for $P<7$. It is strong when it occurs between phase 0·25 and 0·50 but is weak from phase 0·55 to 0·65. The timing of the bump correlates with the time for sound to travel through the envelope: it is earlier when the sound travel time is a smaller fraction of the period and it is later when the sound travel time is greater relative to the period.

It was thus concluded that this feature is a deep-seated property of pulsating stars and depends on the entire envelope structure. It should therefore be a meaningful measure of properties of the star. The sensitivity of the timing of this feature to the parameter Y has only been partially investigated: it appeared insensitive but further study is

warranted. In addition, it has not been excluded that such a feature could appear in an overtone model of significantly different structure. Nevertheless, the present exploration is sufficient to justify using this feature to draw conclusions about the stars where it appears.

It was also found that the calculated limiting amplitude of pulsation correlates with the timing of this feature. When it occurs between phases 0·50 to 0·25 as in the 7- to 10-day Cepheids, the amplitude is only moderate (0·75 magnitude), whereas when the second bump nearly coincides with the first, as it does in Cepheids of 12 or more days' period, it acts to reinforce the pulsation and the limiting amplitude becomes large (about 1·5 magnitude). This behaviour agrees in general with the known amplitude trend of Cepheid variables and this echo mechanism is apparently the explanation of this trend.

It was found that for a given sequence, the value of $V_{0\cdot 83}$ and the timing of the feature was just a function of M/R_0. Since the period depends on M/R_0^3, this permits the adjustment of both M and R_0 in order to match the period and the phase of the feature. A preliminary adjustment has been carried out for β Dor, $P=9^d\cdot 84$. The result was $M=3\cdot 4\,M_\odot$ and $R=54\cdot 5\,R_\odot$. Using a value $T_{e0}=6100$ °K (**17**), this yields $L=3\cdot 7\times 10^3\,L_\odot$ or $M_b=-4\cdot 2$ which is the same as is given by the period luminosity relation.

There are two surprising aspects of this result. First, the mass is only about one-half of the mass that would give the calculated luminosity in an evolutionary model (**18**). This does not mean that the evolutionary model would not show instability but that if the evolutionary model is chosen for a period of 9·84 days, it will not show the secondary bump as observed. This difference in mass can be reconciled with evolutionary calculations provided mass loss (probably in the red giant phase) of about one-half the mass has occurred. This could happen with only slight change in luminosity according to recent calculations (**19**).

The other surprising aspect of this result is the radius. It is only $54\cdot 5\,R_\odot$, whereas Rodgers (**20**), using some very early photometry, has given $105\,R_\odot$. I recalculated this (by the Wesselink method, using additional luminosity data (**21**)) and obtained $69\,R_\odot$. I have also examined my non-linear computed model in some detail to evaluate what the Wesselink method would give if applied to it. I found that the depth of the photosphere is much greater, by 1 per cent of R_0, at maximum radius than at minimum radius so that the value of ΔR appropriate for the photospheric motion is less than that resulting from integrating the velocity curve. This means that in using the ratio of luminosities at equal colour, we arrive at a ratio that is less than the ratio of radii of a definite mass layer which is what is given by integrating the motion as seen in the velocity curve since there is no appreciable

velocity gradient in the photosphere. This correction, only 1 per cent of the radius, is about 10 per cent of ΔR and thereby reduces the calculated radius by about 10 per cent. In this way, my 69 $R_\odot$ would become 62 $R_\odot$. This is not yet a precise measure but this discussion shows that the Wesselink method is subject to significant systematic corrections before its results can be directly used, and my model result of 54·5 $R_\odot$ is not necessarily at variance with observation.

Models with $V_{0.83}$ less than 12·5 have not yet been adequately explored. The single example so far is that of W Vir (**16**) at $V_{0.83}=8{\cdot}7$. The ultimate indication of RV Tauri behaviour that arose in this calculation suggests that this class may be reproduced with values of V in the range <10. Much more exploration of non-linear pulsation is still needed in order to discover all the significant types of behaviour.

Conclusion

Recent work on pulsating variable stars has shown in some detail the mechanisms acting to excite the Cepheid and related types of pulsating variables. The non-linear calculations have begun to make possible the determination of mass, luminosity, radius, and helium content just from examination of observational data on variables. The luminosities so far determined both for RR Lyrae and Cepheid variables are in close agreement with determination by other methods. The masses, however, are persistently lower than evolutionary calculations for Cepheid models and are also lower than usually assumed for RR Lyrae models. It is not yet clear whether any escape from the low mass conclusion can be found but there is no clear contradiction.

This work has been supported in part by the Office of Naval Research Contract [Nonr—220(47)] and the National Aeronautics and Space Administration grant [NsG—426].

REFERENCES

(1) Eddington, A.S., 1917. *Observatory*, **40**, 290.
(2) Eddington, A.S., 1918. *Mon. Not. R. astr. Soc.*, **79**, 2.
(3) Eddington, A.S., 1941. *Mon. Not. R. astr. Soc.*, **101**, 182.
(4) Christy, R.F., 1964. *Rev. mod. Phys.*, **36**, 555.
(5) Christy, R.F., 1966. *Astrophys. J.*, **144**, 108.
(6) Cox, J.P., 1955. *Astrophys. J.*, **122**, 286.
(7) Zhevakin, S.A., 1953. *Russ. Astron. J.*, **30**, 161; 1963. *Ann. Rev. Astr. Astrophys.*, **1**, 367.
(8) Baker, N. & Kippenhahn, R., 1962. *Z. Astrophys.*, **54**, 114.
(9) Cox, J.P., 1963. *Astrophys. J.*, **138**, 487.
(10) Baker, N. & Kippenhahn, R., 1965. *Astrophys. J.*, **142**, 868.
(11) Christy, R.F., 1962. *Astrophys. J.*, **136**, 887.
(12) Cox, A.N., Brownlee, R.R. & Eilers, D.D., 1966. *Astrophys. J.*, **144**, 1024.
(13) Christy, R.F., 1966. *Ann. Rev. Astr. Astrophys.*, **4**, 353.

(14) Christy, R.F., 1967. *Aerodynamic Phenomena in Stellar Atmospheres*, ed. by R.N.Thomas, p. 105, Willmer, Birkenhead.
(15) Cox, J.P., 1967. *Aerodynamic Phenomena in Stellar Atmospheres*, ed. by R.N.Thomas, p. 3, Willmer, Birkenhead.
(16) Christy, R.F., 1966. *Astrophys. J.*, **145**, 337.
(17) Bell, R.A. & Rodgers, A.W., 1967. *Mon. Not. R. astr. Soc.*, **135**, 121.
(18) Hofmeister, E., Kippenhahn, R. & Weigert, A., 1964. *Z. Astrophys.*, **60**, 57.
(19) Forbes, J.E., 1967. Preprint.
(20) Rodgers, A.W., 1957. *Mon. Not. R. astr. Soc.*, **117**, 85.
(21) Mitchell, R.I., Iriarte, B., Steinmetz, D. & Johnson, H.L., 1964. *Ton. Bull.*, **3**, No. 24.
(22) Payne-Gaposchkin, C. & Gaposchkin, S., 1966. *Smithsonian Contr. Ast.*, **9**.